

Extracting Tree-structures in CT data by Tracking Multiple Statistically Ranked Hypotheses

Raghavendra Selvan, Jens Petersen, Jesper H Pedersen, Marleen de Bruijne

Abstract—In this work, we adapt a method based on multiple hypothesis tracking (MHT) that has been shown to give state-of-the-art vessel segmentation results in interactive settings, for the purpose of extracting trees. Regularly spaced tubular templates are fit to image data forming local hypotheses. These local hypotheses are used to construct the MHT tree, which is then traversed to make segmentation decisions. However, some critical parameters in this method are scale-dependent and have an adverse effect when tracking structures of varying dimensions. We propose to use statistical ranking of local hypotheses in constructing the MHT tree, which yields a probabilistic interpretation of scores across scales and helps alleviate the scale-dependence of MHT parameters. This enables our method to track trees starting from a single seed point. Our method is evaluated on chest CT data to extract airway trees and coronary arteries. In both cases, we show that our method performs significantly better than the original MHT method.

Index terms – multiple hypothesis tracking, tree segmentation, CT, airways, vessels

I. INTRODUCTION

Extracting tree structures is a commonly encountered task in image analysis applications. In medical image analysis, reliable methods to extract airways, blood vessels and neuron tracks have important clinical usage. For instance, airway tree extraction is used to study the morphology of airways, which is useful to derive biomarkers for diseases such as chronic obstructive pulmonary disease (COPD) [1], [2] and cystic fibrosis [3]; and segmentation of coronary vessels is useful in prognosis of cardio-vascular diseases [4].

Several methods have been proposed to address tree segmentation tasks occurring in medical images. One general approach is to model local appearance of structures in the tree and the overall connectivity of these local structures. A common local modelling approach is to use templates of the ideal structures of interest and perform template-matching with the image data. This accentuates possible local signals of interest and additional processing on top of such template-matched data can be used to extract the overall connectivity. Multi-scale vesselness filtering is a commonly employed technique to enhance local tubular structures [5]–[7] like vessels and airways. Another simpler approach to detect local structures is to use multi-scale blob detectors [8].

R. Selvan and J. Petersen are with the Department of Computer Science, University of Copenhagen, Denmark

J. H. Pedersen is with the Department of Thoracic Surgery, Rigshospitalet, University of Copenhagen, Denmark

M. Bruijne is with the Department of Computer Science, University of Copenhagen, Denmark and the Biomedical Imaging Group Rotterdam, Departments of Radiology and Medical Informatics, Erasmus MC, Rotterdam, The Netherlands

Template-matching enhances local structures of interest but invariably ends up being noisy. Several classes of methods are used to extract global structures by processing such noisy data. Minimal path methods can be used to extract tree structures by first assigning costs based on template-matching and computing a path of minimum cost via some optimisation scheme. In Wink et al. [9], multi-scale vesselness filter output is transformed into path costs and minimum cost paths are computed using standard algorithm based on Dijkstra [10], yielding candidate vessel centerlines. Another commonly used approach is to employ tracking on top of template-matching. From a signal processing point of view, tracking methods can be seen as powerful denoising techniques that can incorporate strong models. In Selvan et al. [8] Bayesian smoothing is performed, using a Kalman smoother, so as to denoise data from a blob-detector to obtain candidate airway branches. Particle filters have also been used in vessel segmentation applications with template-matching performed at each prediction step [11]. Recent methods involving deep learning, such as in Meng et al. [12] used to extract airways, also take up a similar approach of performing tracking with neural networks used as learnable template functions.

A comprehensive survey of vessel segmentation methods is presented in Lesage et al. [13]. The class of methods we focus on in this contribution are what the authors in Lesage et al. [13] address as template-matching based centerline tracking methods. A comparative study for airway segmentation methods was published in the EXACT’09 study [14], wherein several methods were evaluated on chest CT data. An important take-away from this study has been that there was scope for improvement in extracting missing airway branches. Another interesting point from the study was that more than half of the competing methods used some form of region growing in their segmentation procedure [15]–[18].

In this work, we look at multiple hypothesis tracking (MHT) [19], [20] – a well known decision making paradigm in multi-target tracking – for the purpose of segmenting trees. In methods based on region growing [21] and conventional object tracking [22], segmentation decisions are made instantaneously making them susceptible to local anomalies due to acquisition noise, interfering structures and others. The primary contrasting feature of using MHT is that it is based on deferring decisions to a future step. From any given step, all possible states corresponding to different solutions (local hypotheses) are maintained up to a predefined search depth (global hypotheses) in the form of a hypothesis tree. Decisions about which of the hypotheses to propagate and which ones to prune away at each step are made by tracing

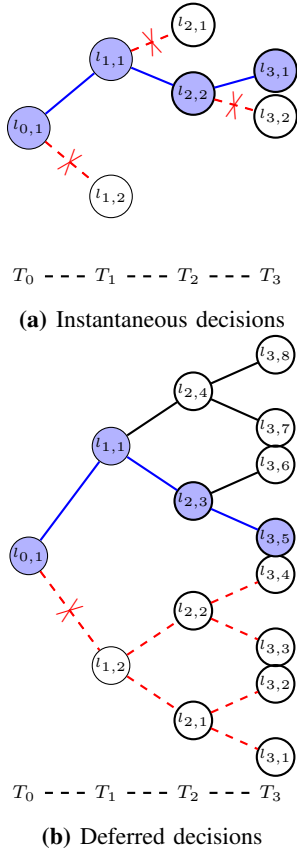


Figure 1: Instantaneous and deferred decisions illustrated using hypothesis trees. Hypothesis trees are shown for tracking steps T_0, \dots, T_3 with local hypothesis i at step t is denoted by $l_{t,i}$. In case of instantaneous decisions in Figure 1a, only the best local hypothesis at each instant is retained (marked in blue). In the case of MHT with search depth 3 in Figure 1b, the decision at T_1 is based on the best global hypothesis at step T_3 , marked with blue edges. Once the decision at T_1 has been made, hypotheses that are not children of the best node are discarded, shown in red.

back the best hypothesis from the end of the hypothesis tree. Such deferred decisions, invariably, take more information into account and make the decisions at any given step more robust than instantaneous ones. The concept of instantaneous and deferred decisions are illustrated in Figure 1.

In the work of Friman et al. [23], MHT was used along with template matching for segmenting small and bright tubular structures from a dark background. This method used in an interactive setting along with minimal paths has remained the best performing method in a coronary vessel segmentation challenge [24], but has not been applied to other tree extraction problems. Critical parameters used to maintain the MHT tree in this method are scale dependent; this has an adverse effect when tracking structures of varying dimensions, such as airway trees. We believe this method has potential to solve a wider range of problems if the limitations with scale dependence can be alleviated.

We introduce statistical ranking of local hypotheses as a means to make local and global hypothesis scores independent of scales. This makes tuning of two crucial MHT parameters easier, allowing us to apply the method to extract trees and/or

structures with branches of varying dimensions without user interaction. The work presented here is based on Friman et al. [23] and an extension of our previously published work [25]. Compared to [25], we present the proposed modifications formally and perform more comprehensive evaluation. We show airway extraction experiments on low-dose CT data from the Danish lung cancer screening trial [26] and segmentation of coronary arteries from CT angiography data from the coronary challenge [24].

II. METHOD

In this section, we present an overview of the method in Friman et al. [23], describe its limitations and present modifications that enable our proposed method to overcome these limitations. For convenience, the method in Friman et al. [23] will be addressed as the original MHT method and ours, with the modifications, as the modified MHT method.

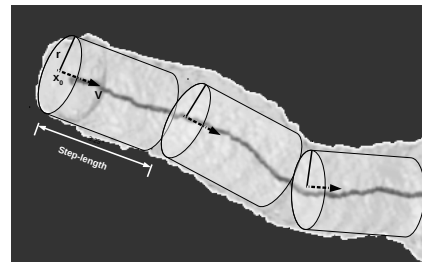


Figure 2: Approximating a structure of interest with a sequence of tubular segments.

A. The original MHT method [23]

The primary objective formulated in the original MHT method is to track bright tubular structures in darker background based on relative contrast of the structures of interest. Tubular structures are modeled as sequences of tubular segments, as depicted in Figure 2, and are segmented by analysing a multiple hypothesis tree comprising template-matched local hypotheses. From each tracking step, several local hypotheses are tested at regular step lengths controlled by the *step length factor* (used as a scaling of the local radius to obtain actual step length). The search span and number of local hypotheses at each step are controlled by the *search angle* and *number of angles* parameters, respectively.

A template function maps cross-sectional intensity variations of a tubular template, of radius r centered at \mathbf{x}_0 along the direction $\hat{\mathbf{v}}$, to a profile function with values between 0 and 1, given as,

$$T(\mathbf{x}; \mathbf{x}_0, \hat{\mathbf{v}}, r) = \frac{r^\gamma}{(d^2(\mathbf{x}; \mathbf{x}_0, \hat{\mathbf{v}}))^{\gamma/2} + r^\gamma}. \quad (1)$$

The steepness of the profile function is controlled by γ and $d^2(\mathbf{x}; \mathbf{x}_0, \hat{\mathbf{v}})$ is the squared distance between any point $\mathbf{x} \in \mathbb{R}^3$ and axis of the tubular template along $\hat{\mathbf{v}}$. We retain the steepness parameter $\gamma = 8$ from Friman et al. [23] and the corresponding profile function is shown in Figure 3.

Next, the image neighbourhood model, $I(\mathbf{x})$, used to fit the image data to the template in Eq. (1) is given as,

$$I(\mathbf{x}) = kT(\mathbf{x}; \mathbf{x}_0, \hat{\mathbf{v}}, r) + m + \epsilon(\mathbf{x}), \quad (2)$$

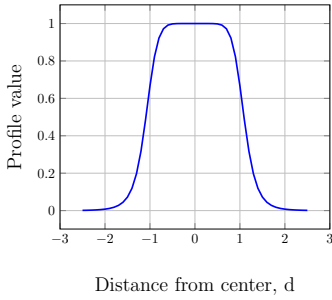


Figure 3: Tubular templates are mapped to profile functions shown here.

where $\epsilon(\mathbf{x})$ captures noise which could be due to interfering structures, image artifacts or acquisition noise, k is the contrast and m is the mean intensity. Template fitting is carried out by solving the following weighted least-squares problem:

$$\operatorname{argmin}_{k,m,r,\mathbf{x}_0,\hat{\mathbf{v}}}\|\mathbf{W}(r,\mathbf{x}_0,\hat{\mathbf{v}})[kT(\mathbf{x}_0,\hat{\mathbf{v}},r)+m\mathbf{1}_n-\mathbf{I}]\|^2, \quad (3)$$

where $\mathbf{W}(r,\mathbf{x}_0,\hat{\mathbf{v}})$ is a weighting function with diagonal entries corresponding to an asymmetric Gaussian centered at \mathbf{x}_0 . It is used to localise the fitting procedure and \mathbf{I} is the image data with non-zero weights under this weighting function. The width of the weighting function is controlled by the *weight window* parameter. We refer to the original paper [23] for details on the weighting matrix and the procedure to solve this minimisation problem, which is carried out using the Levenberg-Marquardt algorithm.

By solving the minimisation problem in Eq. (3) for several local hypotheses at each step, estimates of tubular template parameters – $r, \mathbf{x}_0, \hat{\mathbf{v}}$ – and of image parameters – k, m – are obtained. The fit of each local hypothesis, i , is quantified using the local hypothesis score, l_i , by computing the Student distribution’s t-statistic:

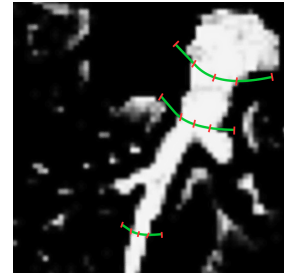
$$l_i \triangleq \frac{k-m}{\operatorname{std}(k)}. \quad (4)$$

The local hypothesis score gives a measure of how significantly different the bright tubular structure is from its background, which can be interpreted as the contrast signal-to-noise ratio (SNR). Local hypotheses below a threshold, referred to as the *local threshold*, are discarded to control the number of candidate hypotheses. Further, a hypothesis tree of a predetermined search depth, d , is constructed using local hypotheses from each step. A sequence of local hypothesis of length d forms a global hypothesis with an aggregated score,

$$s_g = \frac{\sum_{i=1}^d l_i}{d}. \quad (5)$$

This score is compared with the *global threshold* and all global hypotheses that do not exceed this threshold are discarded.

Overall, two categories of parameters are used to tune the original MHT method. First category of parameters are related to generating local hypotheses: minimum and maximum radii, step length factor between successive tracking steps, window of the weighting function, maximum search angle and number of local hypotheses at each step. Second category of parameters are used to control the MHT behaviour: search depth, local



Org. MHT	Mod. MHT
(0.7, 2.1, 9, 4, 0.5)	(0.25, 0.33, 1, 0.50, 0.20)
(0.1, 3.2, 5, 2, 0.3)	(0.20, 0.50, 1, 0.33, 0.25)
(0.2, 0.4, 2, 1, 0.1)	(0.25, 0.33, 1, 0.50, 0.20)

Figure 4: Illustration of a branch of varying dimensions along with the local hypothesis scores for the original and modified MHT methods. Notice how the scores of the best hypothesis at each scale varies for the original MHT method.

and global thresholds. We again refer to Friman et al. [23] for elaboration on the role of these parameters.

B. Modifications to the original MHT method

The original MHT method was devised as an interactive method to track tubular structures. It is not immediately applicable for the automatic extraction of trees with branches of varying dimensions. In this section, some limitations of the original MHT method in this regard are elaborated and modifications are proposed to overcome them.

1) *Dealing with scale-dependence:* An important factor to consider when tracking tree-structures with branches of varying dimensions is their range. With airway trees for instance, the radius of visible airways in CT typically ranges from 1mm to 10mm. When using the original MHT method, such variations make it hard to obtain optimal parameter settings across scales. This behaviour is demonstrated for local hypothesis scores, computed using Eq. (4), in Figure 4. Specifically, local hypothesis scores tend to decrease with scale, making it challenging to obtain a single optimal local threshold that works well across scales. When the local threshold is tuned to extract smaller branches, then the chance of adding large and sub-optimal branches to the hypothesis tree is higher resulting in over-segmentation. Similarly, when the score is tuned for larger branches even the best candidate hypothesis for smaller branches might not qualify as valid candidates resulting in under-segmentation.

To alleviate the aforementioned scale dependence, we devise a strategy of ranking local hypotheses based on their scores. Instead of using the scores in Eq. (4) directly, we sort them in decreasing order to derive a ranking based score at each step in the range $[0, 1]$. If N local hypotheses are sampled at any given step, then the scores of the ranked local hypotheses are obtained as,

$$l'_i = \frac{1}{R_i} \quad \forall i \in 1 \dots N, \quad (6)$$

where $R_i \in \{1, \dots, N\}$ is the rank of the N local hypotheses. By this scheme of relative scoring of hypotheses, where the best local hypothesis is assigned 1 at each tracking step, the problem of scale dependence of hypothesis scores is

immediately alleviated. This is demonstrated in the table to the right in Figure 4.

A useful interpretation of such a ranking is to see it as a measure of the relative significance of local hypotheses at each step. When aggregated over the depth of the tree, it can be interpreted as the likelihood of the corresponding global hypothesis. Consider an example when the search depth is 10 and the global hypothesis threshold is 0.6. For a global hypothesis (comprising of a sequence of 10 local hypotheses) to score above 0.6 it would require its component local hypotheses to have been best locally at least in 6 of the 10 tracking steps, on average. This relative significance provides a probabilistic global hypothesis score, making it independent of the scale and variations of structures and removes the need to perform two level pruning of hypotheses – using local and global hypothesis thresholds – as done in the original MHT method. Instead of explicitly pruning local hypotheses, we propagate all local hypotheses with their ranked scores from Eq. (6) and rely on the deferred decisions of MHT algorithm to yield valid branches. That is, the search depth of the MHT tree and global threshold are the only critical parameters; in effect, removing the local threshold parameter.

One possible concern that arises when the scores in Eq. (4) are discarded for relative ranking in Eq. (6) is the chance of poor candidate hypotheses performing well when ranked amongst equally poor counterparts. A strength of the deferred decision of MHT is that with adequate depth of the MHT tree such hypotheses are unlikely to be accepted, as they would have to perform well across multiple steps.

2) *Handling branching*: Another factor to consider when tracking trees is branching. In the original MHT method, bifurcation detection is performed by clustering hypotheses based on their spatial location at every step using a spectral clustering algorithm [27]. However, there are no further details as to how the MHT tree is maintained after bifurcations. Once a bifurcation is detected, there are several ways to proceed. As the tracking happens per branch, new seed points can be added from the detected points of bifurcation and tracking can be restarted. This entails rebuilding of the MHT tree from each of the new seed points. The implementation of the original MHT method, available as a MeVisLab¹ module, follows this strategy. This has a negative consequence of discarding the information aggregated until the step before branching.

Another strategy that does not rely on rebuilding the MHT tree is to simply save the MHT tree at branching and resume tracking from each of the newly detected branching points separately. By resuming tracking from both branching points with the history of the parent branch we do not throw away information. In our modified MHT method, this strategy is used.

III. EXPERIMENTS AND RESULTS

We evaluate the modified MHT method for two applications: extraction of airway trees and segmentation of coronary arteries. We used the MeVisLab implementation of the original MHT method for performing the original MHT experiments

¹<http://mevislab.de/>

and a customised module with our modifications on MeVisLab for the modified MHT method. Details of preprocessing of data, experiments, error measures and results are presented next.

A. Airway tree extraction from lung CT

Experiments were performed on a subset of 32 low-dose CT scans from the Danish Lung Cancer Screening Trial [26] dataset. The 3D images in this dataset have a slice spacing of 1 mm and in-plane resolution varying between 0.72 to 0.78 mm. The images were randomly split into training and test sets comprising of 16 images each. Performance of the method was compared with reference segmentations composed of an expert-corrected union of two previous methods: the first method uses an appearance model based on a voxel classifier to distinguish airway voxels from background and uses region growing along with a vessel similarity measure to extract airways [21], and the second method uses a similar voxel classifier but extracts airways by continually extending locally optimal paths [28].



Figure 5: Maximum intensity projection view of the probability image obtained from the voxel-classifier. Brighter regions correspond to higher probability, and hence more likely to belong to airways.

1) *Pre-processing of data*: All CT images were pre-processed and converted into probability images using a kNN-based voxel classifier trained to distinguish airway voxels from background [21]. Thus obtained probability images have probability close to 1 in regions that are classified to be inside the airways and close to 0 outside; these images match the profile function described in Section II, wherein, the structure of interest is bright (high probability) in a dark background. An example probability image is shown in Figure 5. Noise in the image is due to several factors including acquisition, interfering vessels, ribs and lung tissue.

2) *Error measure*: Performance of all four methods are evaluated based on accuracy of the extracted centerlines. To standardise the evaluation procedure, centerlines were extracted from the binary segmentations from all methods using a 3D thinning algorithm [29]. The error measure is a symmetric distance between extracted and reference centerlines, given as,

$$d_{err} = w \frac{\sum_{i=1}^{n_{op}} \min d_E(c_i, C_{ref})}{n_{op}} + (1 - w) \frac{\sum_{j=1}^{n_{ref}} \min d_E(c_j, C_{op})}{n_{ref}}. \quad (7)$$

Table I: Optimal parameters for both MHT methods (Org. and Mod.) based on training set for airway extraction along with the search range of parameters. Parameters with * were fixed based on the morphology of airways and *Search depth* was fixed based on initial experiments. ⁺ We refer to the text in Section III-A3 for explanation on *Global threshold* for the original MHT method, and to Section ?? for two different ranges for *Weight window*.

Parameter/Method	Search Range	Org.	Mod.
Min. radius* (mm)	1	1	1
Max. radius* (mm)	10	10	10
Step length	[1.0, 1.1, ..., 2.0]	1.5	1.1
Weight window ⁺	[3, 4, 5] / [1, 2, ..., 5]	3.0	1.0
Search depth	6	6	6
Search angle (deg.)	[30, 40, ..., 70]	60	70
Number of angles	[1, 2, ..., 5]	3	2
Local thres.(T_{loc})	[1.0, 2.0, ..., 5.0]	2.0	–
Global thres. ⁺	$2T_{loc} / [0.5, 0.6, ..., 0.9]$	4.0	0.7

In the above equation, C_{ref} , C_{op} are set of equidistant points on the centerlines of the reference and output segmentation results, respectively, comprising of n_{ref} and n_{op} number of points. $c_i, c_j \in \mathbb{R}^n$ are individual points on the centerlines, d_E is the Euclidean distance and w is a weight, such that $0 \leq w \leq 1$. Notice that the first term in Eq. (7) captures the distance between the two centerlines due to false positives, whereas the second term captures the distance due to false negatives. In this work we use $w = 0.5$. Depending on the application the weight can be modified to obtain a desirable measure that reflects the sensitivity or specificity needs.

3) *Experiment set-up and parameter tuning:* The modified MHT method was compared to the original MHT method and with region growing applied to both the probability and intensity images. Parameters of all the methods were tuned on the training set comprising 16 images and tested on an independent test set consisting of 16 images. Both the MHT methods have tunable parameters; the first set of parameters is related to the tubular template: minimum and maximum allowable radii of the templates, scaling factors for step length and weight window. A second category of parameters is related to multiple hypothesis tracking: search depth, search angle, number of angles, local and global hypothesis thresholds. Tuning both categories of parameters for the training set is cumbersome, so the minimum and maximum radii were fixed to 1mm and 10mm, respectively, based on prior knowledge about the morphology of airway trees. Also the search depth parameter was set to 6 for both methods based on initial experiments. Only the remaining parameters were tuned to minimise the training error defined in Eq. (7) using grid search. The range of parameters searched over and the optimal set of parameters obtained for both MHT methods are summarised in Table I. Due to the scale independence introduced by the statistical ranking of local hypotheses, the modified MHT method does not have the local threshold as a parameter. The range of parameters for global threshold shown is for the modified MHT method, as the global threshold for the original MHT method was always set to be twice the optimal local threshold based on Friman et al. [23]. Both region growing methods only have the threshold parameter to be tuned. The optimal threshold for region growing on intensity of

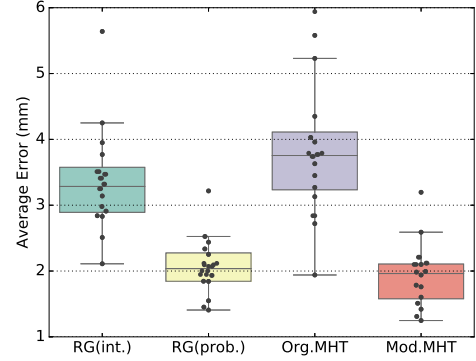


Figure 6: Average error on 16 scans in the test set to compare the modified MHT method with region growing (RG) on intensity images, region growing on probability images and the original MHT method, visualised as standard box plots. Both MHT methods were applied to the probability images.

CT images was found to be -995 HU which is a low threshold, due to the leakage for three images in the training set for any higher thresholds. The optimal threshold for the case of probability images based on the training set performance was found to be 0.5. All four methods require an initial seed point and the same seed point in the trachea, automatically extracted using the procedure described in Lo et al. [21], was provided to all.

We use the MHT module in MeVisLab provided by the authors in Friman et al. [23] to perform the original MHT experiments. In this implementation, minimum value for the weight window factor is constrained to be 3. However, for the modified MHT method we tried a larger range $[1, 2, \dots, 5]$, and found the training error to be slightly lower (by 0.2mm) when compared to using the smaller range $[3, 4, 5]$. We adhere to using this larger range for modified MHT method, and a smaller range for original MHT method, also for the Coronary Artery Extraction experiments.

Table II: Average error comparison for extraction of airways

Method	d_{err} (mm)
RG (intensity)	3.368 ± 0.808
RG (probability)	2.064 ± 0.447
Original MHT	3.961 ± 1.384
Modified MHT	1.929 ± 0.494

4) *Results:* Performance comparison was based on computing the average error measure in Eq. (7) and results for the test set are presented in Table II and visualised in Figure 6. Differences between methods were tested for statistical significance using paired sample t -tests. The modified MHT method clearly shows an improvement when compared to the original MHT method ($p < 0.001$) and region growing on intensity images ($p < 0.001$), but was not significantly better than region growing on probability images ($p = 0.079$). Six of the test set results for the modified MHT method are visualised in Figure 7 along with the reference segmentations.

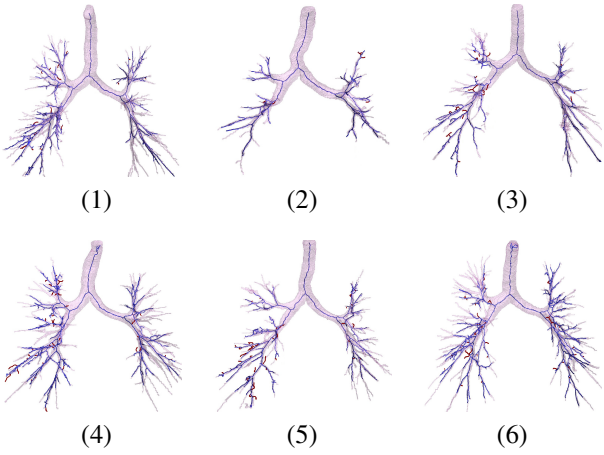


Figure 7: Six test case centerline results (thick lines) from the modified MHT method are shown overlaid on the reference segmentations (background surface). True positive portion of the extracted centerline is shown in blue and false positive portion in red.

B. Coronary Artery Extraction

We next describe experiments on 3D CT angiography (CTA) images for segmenting coronary arteries evaluated on the Coronary Artery Challenge data². The challenge organisers allow methods to compete in three categories based on the extent of user interaction per vessel: automatic (no seed points), semi-automatic (one seed point) and interactive (more than one seed point). A version of the original MHT method, used along with a minimal path algorithm used in an interactive setting [23], [30], has remained the best performing method in the Coronary Artery Challenge [24]. We evaluate the original and modified MHT methods as stand-alone, semi-automatic methods and compare to the results of Friman et al. [23].

1) *Data and preprocessing:* The dataset consists of 32 CTA images, split into 8 images for training and the remaining 24 for testing. These 3D volumes have a mean voxel size of $0.32 \times 0.32 \times 0.4 \text{ mm}^3$.

The objective of the challenge is to segment four vessels per dataset. To this end, four seed points per vessel are provided, of which one must be selected for semi-automatic methods:

- Point S: start point of centerline
- Point E: end point of centerline
- Point B: a point about 3cm distal of the start point along the centerline
- Point A: a point inside distal part of the vessel.

In all images, three of the four vessels to be segmented were of the same type: right coronary artery (RCA), left anterior descending artery (LAD) and left circumflex artery (LCX). The fourth vessel, however, varied between images and was one of the large side branches (LSB). The reference standard for the training set was provided as manually drawn centerlines.

We closely adhere to the preprocessing performed in the original MHT method [23], [30]. Unsigned integers are used to represent the voxel intensities as gray value (GV), under

a simple transformation of the corresponding Hounsfield Unit (HU): $HU(\mathbf{x}) = GV(\mathbf{x}) - 1024$. To enable improved vessel template matching, voxel intensity of the lung tissue is raised to that of myocardial tissue and vessel calcifications are eliminated with the following thresholds:

$$I(\mathbf{x}) = \begin{cases} t_{myo} & \text{if } I(\mathbf{x}) < t_{myo} \\ I(\mathbf{x}) & \text{if } t_{myo} \leq I(\mathbf{x}) \leq t_{calc} \\ t_{myo} & \text{if } I(\mathbf{x}) > t_{calc}, \end{cases} \quad (8)$$

with $t_{myo} = 950$ and $t_{calc} = 1700$.

2) *Error measure:* We use two commonly reported measures on the challenge website in our evaluations, that quantify completeness and accuracy of the segmented vessels, defined as OV (overlap) and AI (average distance inside vessel) in Schaap et al. [24], respectively.

Table III: Optimal parameters for both MHT methods after tuning on the training set for Coronary Artery Challenge to maximise overlap (OV) along with the search range of parameters. Parameters with * were fixed based on the morphology of vessels and *Search depth* was fixed based on initial experiments.

⁺ We refer to the text in Section III-B3 for explanation on *Global threshold* for the original MHT method and two different ranges for *Weight window*.

Parameter/Method	Search range	Org.	Mod.
Min. radius* (mm)	1	1	1
Max. radius* (mm)	3	3	3
Search depth	4	4	4
Weight Window ⁺	[3, 4, 5] / [1, 2, ..., 5]	3	1
Step Length	[1.0, 1.1, ..., 2.0]	1.5	1.5
Search Angle (deg.)	[30, 40, ..., 70]	60	60
Number of angles	[1, 2, ..., 5]	3	2
Local Thres. (T_{loc})	[1.0, 2.0, ..., 5.0]	4.0	-
Global Thres. ⁺	$2T_{loc}$ / [0.55, 0.65, ..., 0.95]	8.0	0.95

3) *Experiment set-up and parameter tuning:* As with the airway tree extraction experiments in Section III-A3, most of the parameters are tuned for both MHT methods, while some are fixed based on prior knowledge. The minimum and maximum radii parameters are set to 1mm and 3mm, respectively. *Search depth* was set to 4 based on initial experiments. Remaining parameters are tuned to maximise overlap, OV, on the training set and are summarised in Table III. Further, as with the airway experiments, the starting value of weight window factor is 3, and the global threshold is twice the local threshold, for the original MHT method. Due to the varying quality of images across the training set, tracking from different seed points yields substantially different results. Based on the training starting tracking from Point B and tracking in both directions turned out to be most useful for both MHT methods.

4) *Results:* We compare the modified MHT method with the original MHT method, evaluated as semi-automatic methods in the ongoing Coronary Artery Challenge evaluation. The modified MHT method scored 91.8% overlap and accuracy of 0.38mm, whereas the original MHT method obtained 67.6% overlap and accuracy of 0.39mm. There is significant improvement in overlap when compared to the original MHT method ($p < 0.001$) as indicated by a paired sample *t*-test. With these results our method stands as the third best performing method

²<http://coronary.bigr.nl/centerlines/index.php>

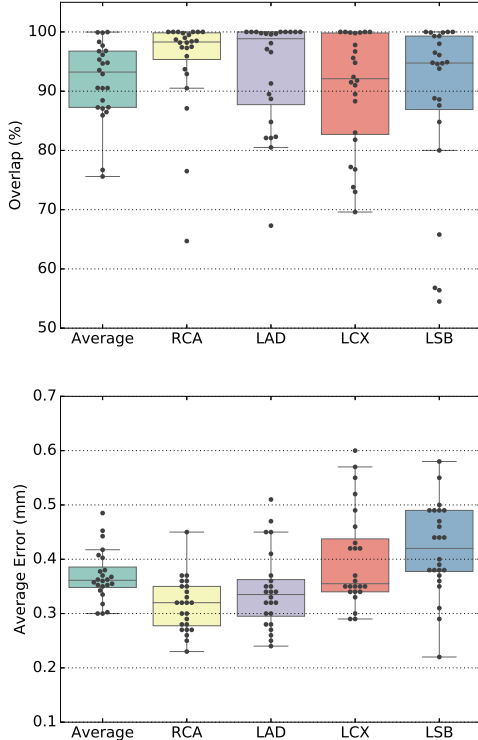


Figure 8: Overlap (OV) and accuracy (AI) measures for the modified MHT method evaluated on the coronary challenge test set.

amongst all semi-automatic methods (requiring one seed point) reported on the challenge website.

Table IV: Overlap (OV) and accuracy (AI) for the original MHT method as interactive and semi-automatic methods, and the modified MHT method.

Method	OV(%)	AI (mm)
Org. MHT (interactive) [23]	98.521 ± 2.183	0.230 ± 0.055
Org. MHT (semi-automatic)	67.612 ± 13.334	0.388 ± 0.066
Modified MHT	91.783 ± 6.630	0.368 ± 0.047

Test set measures for each of the four vessels, along with the average score per dataset, are shown in Figure 8 for the modified MHT method. The first plot in Figure 8 shows the overlap performance and it is clear that RCA, LAD and LCX vessels score high consistently and have few outliers. LSB, on the other hand, has four cases scoring less than 70% in OV. One possible reason is that the vessel chosen as LSB was different across the dataset and the tuned parameters could not generalise to these four cases. The second plot in Figure 8 depicts the accuracy (AI) for the test set across the four vessels and again the average error in LSB is slightly higher than the rest. In Table IV we summarise the results for two versions of the original MHT method and the modified MHT method.

IV. DISCUSSION AND CONCLUSIONS

In this work, we extended the template-matching based centerline extraction method using multiple hypothesis tracking presented in Friman et al. [23]. We introduced statistical

ranking of local hypotheses as a possible means to overcome scale dependence of important MHT parameters. Two such parameters (local and global thresholds that are scale dependent) make the original MHT method less useful for tracking structures of varying dimensions. Due to the proposed changes the modified MHT method can now be considered semi-automatic, requiring only one seed point per tree. In most cases, even the one required seed point can also be automatically provided, as done in case of airways in Lo et al. [21], and thus making the method fully automatic. We also presented an improvement to the bifurcation handling strategy by maintaining the history of the MHT tree across bifurcations instead of restarting tracking at bifurcation points.

We presented evaluations in Section III, where we first focussed on extracting airway trees from chest CT data, and compared the modified MHT method with region growing on intensity images, region growing on probability images and the original MHT method. The modified MHT method shows significant improvement in average centerline distance when compared to the original MHT method ($p < 0.001$).

We also presented evaluations on the Coronary Challenge [24] and compared the modified MHT method with the original MHT method used as a semi-automatic method. The interactive version of the original MHT method, which is a combination of MHT, minimal paths and extensive user interaction (on average 1.5 clicks per vessel), is still the best performing method in the Coronary Artery Challenge. The modified MHT method, however, shows significant improvement in the overlap measure (OV) when compared to the semi-automatic original MHT method ($p < 0.001$). The accuracy of the extracted centerlines (AI) from both semi-automatic versions of the MHT method are close, indicating that the original MHT method (used semi-automatically) was accurate in the vessels that were segmented, but it under-segments the vessels indicated by the low OV score. This is likely due to dependence of the parameters on scale, which is overcome with the statistical ranking introduced in the modified MHT method. In this work we evaluated the modified MHT method using one seed point per vessel for the gains in some of the cases, while still competing in the semi-automatic category of the challenge. However, the modified MHT method could also have been used with fewer than one seed point per vessel (one seed point per tree) and yielding similar performance, as we were able to extract substantial portions of the coronary tree starting from a single seed point.

There are two recent semi-automatic methods based on diffusion tensor imaging techniques [31], [32] that perform better than the modified MHT method in the OV measures as reported in the challenge website with a score of 97.3% and 96.4%, respectively. Three other methods in the fully automatic category have better OV measure by a small margin, between 1 – 2%, when compared to the modified MHT method [6], [7], [33]. One common feature across all these better performing methods is the pre-processing performed on the CT images to enhance vessel-like structures. For instance, in the currently best performing fully automatic method an improved version of Frangi’s vesselness is used before centerline extraction [7], and similarly in Bauer et al. [6] a tube

detection filter is used and a pre-trained vessel detection filter is used in Zheng et al. [33]. In the modified MHT method we use a simple template-matching step and, use of more sophisticated strategies as described in the other methods in the challenge should further improve the performance. For instance, we expect that the use of probability images obtained from a voxel classifier to distinguish vessel and non-vessel voxels instead of intensity images, as in the case of the airway experiments, could have been beneficial.

In conclusion, we proposed modifications to the well established original MHT method that yield significantly better results. Statistical ranking of local hypotheses yields a common interpretation of the global hypotheses of the MHT tree at all scales. The proposed modifications also make it possible to use the method in a non-interactive manner and yield competitive results on versatile datasets involving segmentation of complete tree structures.

Acknowledgements

This work was funded by the Independent Research Fund Denmark (DFF) and Netherlands Organisation for Scientific Research (NWO).

REFERENCES

- [1] Y. Nakano, S. Muro, H. Sakai, T. Hirai, K. Chin, M. Tsukino, K. Nishimura, H. Itoh, P. D. Paré, J. C. Hogg *et al.*, “Computed tomographic measurements of airway dimensions and emphysema in smokers: correlation with lung function,” *American journal of respiratory and critical care medicine*, vol. 162, no. 3, pp. 1102–1108, 2000.
- [2] M. Hasegawa, Y. Nasuhara, Y. Onodera, H. Makita, K. Nagai, S. Fuke, Y. Ito, T. Betsuyaku, and M. Nishimura, “Airflow limitation and airway dimensions in chronic obstructive pulmonary disease,” *American journal of respiratory and critical care medicine*, vol. 173, no. 12, 2006.
- [3] W. Kuo, M. de Bruijne, J. Petersen, K. Nasserinejad, H. Ozturk, Y. Chen, A. Perez-Rovira, and H. A. Tiddens, “Diagnosis of bronchiectasis and airway wall thickening in children with cystic fibrosis: Objective airway-artery quantification,” *European Radiology*, pp. 1–10, 2017.
- [4] W. Rosamond, K. Flegal, K. Furie, A. Go, K. Greenlund, N. Haase, S. M. Hailpern, M. Ho, V. Howard, B. Kissela *et al.*, “Heart disease and stroke statistics—2008 update,” *Circulation*, vol. 117, no. 4, pp. e25–e146, 2008.
- [5] A. F. Frangi, W. J. Niessen, K. L. Vincken, and M. A. Viergever, “Multi-scale vessel enhancement filtering,” in *International Conference on Medical Image Computing and Computer-Assisted Intervention*. Springer, 1998, pp. 130–137.
- [6] C. Bauer and H. Bischof, “Edge based tube detection for coronary artery centerline extraction,” *The Insight Journal*, 2008.
- [7] G. Yang, P. Kitslaar, M. Frenay, A. Broersen, M. J. Boogers, J. J. Bax, J. H. Reiber, and J. Dijkstra, “Automatic centerline extraction of coronary arteries in coronary computed tomographic angiography,” *The international journal of cardiovascular imaging*, vol. 28, no. 4, 2012.
- [8] R. Selvan, J. Petersen, J. H. Pedersen, and M. de Bruijne, “Extraction of airways with probabilistic state-space models and Bayesian smoothing,” in *Graphs in Biomedical Image Analysis, Computational Anatomy and Imaging Genetics*. Springer, 2017, pp. 53–63.
- [9] O. Wink, W. J. Niessen, and M. A. Viergever, “Multiscale vessel tracking,” *IEEE Transactions on Medical Imaging*, vol. 23, no. 1, pp. 130–133, 2004.
- [10] E. W. Dijkstra, “A note on two problems in connexion with graphs,” *Numerische mathematik*, vol. 1, no. 1, pp. 269–271, 1959.
- [11] C. Florin, N. Paragios, and J. Williams, “Particle filters, a quasi-monte carlo solution for segmentation of coronaries,” in *International Conference on Medical Image Computing and Computer-Assisted Intervention*. Springer, 2005, pp. 246–253.
- [12] Q. Meng, H. R. Roth, T. Kitasaka, M. Oda, J. Ueno, and K. Mori, “Tracking and segmentation of the airways in chest CT using a fully convolutional network,” in *International Conference on Medical Image Computing and Computer-Assisted Intervention*. Springer, 2017.
- [13] D. Lesage, E. D. Angelini, I. Bloch, and G. Funka-Lea, “A review of 3D vessel lumen segmentation techniques: Models, features and extraction schemes,” *Medical image analysis*, vol. 13, no. 6, pp. 819–845, 2009.
- [14] P. Lo, B. Van Ginneken, J. M. Reinhardt, T. Yavarna, P. A. De Jong, B. Irving, C. Fetita, M. Ortner, R. Pinho, J. Sijbers *et al.*, “Extraction of airways from CT (EXACT’09),” *IEEE Transactions on Medical Imaging*, vol. 31, no. 11, pp. 2093–2107, 2012.
- [15] M. Feuerstein, T. Kitasaka, and K. Mori, “Adaptive branch tracing and image sharpening for airway tree extraction in 3-d chest ct,” in *Proc. Second International Workshop on Pulmonary Image Analysis*, 2009.
- [16] C. Bauer, T. Pock, H. Bischof, and R. Beichel, “Airway tree reconstruction based on tube detection,” in *Proc. of Second International Workshop on Pulmonary Image Analysis*, 2009, pp. 203–213.
- [17] R. Wiemker, T. Bülow, and C. Lorenz, “A simple centrality-based region growing algorithm for the extraction of airways,” in *Proc. Second International Workshop on Pulmonary Image Analysis (MICCAI)*. Citeseer, 2009, pp. 309–314.
- [18] J. Lee and A. P. Reeves, “Segmentation of the airway tree from chest CT using local volume of interest,” in *Proc. of Second International Workshop on Pulmonary Image Analysis*, 2009, pp. 273–284.
- [19] D. Reid, “An algorithm for tracking multiple targets,” *IEEE transactions on Automatic Control*, vol. 24, no. 6, pp. 843–854, 1979.
- [20] S. S. Blackman, “Multiple hypothesis tracking for multiple target tracking,” *IEEE Aerospace and Electronic Systems Magazine*, vol. 19, no. 1, pp. 5–18, 2004.
- [21] P. Lo, J. Sporring, H. Ashraf, J. J. Pedersen, and M. de Bruijne, “Vessel-guided airway tree segmentation: A voxel classification approach,” *Medical image analysis*, vol. 14, no. 4, pp. 527–538, 2010.
- [22] T. Yedidya and R. Hartley, “Tracking of blood vessels in retinal images using Kalman filter,” in *Computing: Techniques and Applications, 2008. DICTA’08. Digital Image*. IEEE, 2008, pp. 52–58.
- [23] O. Friman, M. Hindennach, C. Kühnel, and H.-O. Peitgen, “Multiple hypothesis template tracking of small 3D vessel structures,” *Medical image analysis*, vol. 14, no. 2, pp. 160–171, 2010.
- [24] M. Schaap, C. T. Metz, T. van Walsum, A. G. van der Giessen, A. C. Weustink, N. R. Mollet, C. Bauer, H. Bogunović, C. Castro, X. Deng *et al.*, “Standardized evaluation methodology and reference database for evaluating coronary artery centerline extraction algorithms,” *Medical image analysis*, vol. 13, no. 5, pp. 701–714, 2009.
- [25] R. Selvan, J. Petersen, J. H. Pedersen, and M. de Bruijne, “Extraction of airway trees using multiple hypothesis tracking and template matching,” in *The Sixth International Workshop on Pulmonary Image Analysis*. CreateSpace Independent Publishing Platform, 2016.
- [26] J. H. Pedersen, H. Ashraf, A. Dirksen, K. Bach, H. Hansen, P. Toennesen, H. Thorsen, J. Brodersen, B. G. Skov, M. Døssing *et al.*, “The Danish randomized lung cancer CT screening trial—overall design and results of the prevalence round,” *Journal of Thoracic Oncology*, vol. 4, no. 5, pp. 608–614, 2009.
- [27] F. R. Chung, *Spectral graph theory*. American Mathematical Soc., 1997, no. 92.
- [28] P. Lo, J. Sporring, J. J. H. Pedersen, and M. de Bruijne, “Airway tree extraction with locally optimal paths,” in *International Conference on Medical Image Computing and Computer-Assisted Intervention*. Springer, 2009, pp. 51–58.
- [29] T.-C. Lee, R. L. Kashyap, and C.-N. Chu, “Building skeleton models via 3-D medial surface axis thinning algorithms,” *CVGIP: Graphical Models and Image Processing*, vol. 56, no. 6, pp. 462–478, 1994.
- [30] O. Friman, C. Kühnel, and H.-O. Peitgen, “Coronary centerline extraction using multiple hypothesis tracking and minimal paths,” in *International Conference on Medical Image Computing and Computer-Assisted Intervention*, vol. 42, 2008.
- [31] S. Cetin, A. Demir, A. Yezzi, M. Degertekin, and G. Unal, “Vessel tractography using an intensity based tensor model with branch detection,” *IEEE transactions on medical imaging*, vol. 32, no. 2, pp. 348–363, 2013.
- [32] S. Cetin and G. Unal, “A higher-order tensor vessel tractography for segmentation of vascular structures,” *IEEE transactions on medical imaging*, vol. 34, no. 10, pp. 2172–2185, 2015.
- [33] Y. Zheng, H. Tek, and G. Funka-Lea, “Robust and accurate coronary artery centerline extraction in CTA by combining model-driven and data-driven approaches,” in *International Conference on Medical Image Computing and Computer-Assisted Intervention*. Springer, 2013.